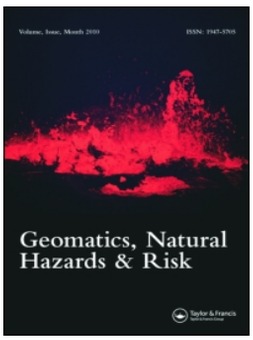

Geomatics, Natural Hazards and Risk

ISSN: 1947-5705 (Print) 1947-5713 (Online) Journal homepage: https://www.tandfonline.com/loi/tgnh20

A detailed *b*-value and fractal dimension study of the March 1999 Chamoli earthquake (M_s 6.6) aftershock sequence in western Himalaya

Arnab Ghosal , Uma Ghosh & J.R. Kayal

To cite this article: Arnab Ghosal , Uma Ghosh & J.R. Kayal (2012) A detailed *b*-value and fractal dimension study of the March 1999 Chamoli earthquake (M_s 6.6) aftershock sequence in western Himalaya, Geomatics, Natural Hazards and Risk, 3:3, 271-278, DOI: 10.1080/19475705.2011.627380

To link to this article: https://doi.org/10.1080/19475705.2011.627380

Published online: 22 Dec 2011.

Geomatics, Natural Hazards and Risk
Vol. 3, No. 3, August 2012, 271–278

Taylor & Francis
Taylor & Francis Group

A detailed *b*-value and fractal dimension study of the March 1999 Chamoli earthquake (M_s 6.6) aftershock sequence in western Himalaya

ARNAB GHOSAL†, UMA GHOSH‡‡ and J.R. KAYAL§
†Indian School of Mines, Dhanbad 826004, India
‡‡Lalbaba College (Calcutta University), Belur, Howrah 711202, India
§Jadavpur University, Kolkata 700032, India

(*Received 26 August 2011; in final form 23 September 2011*)

The aftershock sequence of the March 1999 Chamoli earthquake (M_s 6.6) in the western Himalaya is analysed to examine the seismic characteristics of the active fault. About 350 aftershocks recorded by about 40 seismic stations are used to map the *b*-value and fractal correlation dimension (D_c) in the earthquake source area. The maximum likelihood method is used to estimate the *b*-value, and the correlation integral method for the fractal correlation dimension. A comparatively higher *b*-value (0.7) is mapped to the north at the Main Central Thrust (MCT) zone with respect to a lower *b*-value (0.5) to the south at the Alakananda fault (ANF) zone. The cross section of the *b*-value imaged the seismically active ANF at depth. The fractal dimension map, on the other hand, identified the ANF with $D_c \sim 0.8$–0.9, that implies a near linear seismogenic structure at the ANF.

1. Introduction

The Chamoli earthquake occurred on March 29, 1999 in the Chamoli district, Garhwal tectonic block of the Main Himalayan Seismic Belt (MHSB) in western Himalaya (figure 1). The magnitude of the earthquake was estimated at between M_s 6.6 and M_L 6.8, the epicentre located at 30.512°N, 79.403°E and the focal depth at $\sim$15 km (IMD 2000). The maximum intensity was reported to be VII (MSK) which was delimited by the Alakananda fault (GSI 2001). In addition to the network of eight permanent stations in the Garhwal Himalaya, various national organizations such as the Geological Survey of India (GSI), India Meteorological Department (IMD), Wadia Institute of Himalayan Geology (WIHG), National Geophysical Research Institute (NGRI), Delhi University and the Indian Institute of Technology - Roorkee (IIT-R) deployed temporary seismic stations to monitor the aftershocks for about 3 months immediately after the main shock. In total about 40 stations were in operation for monitoring aftershocks. Seismotectonics of the Chamoli earthquake sequence was reported by Kayal *et al.* (2003a). Based on the local permanent network data ($M > 2.5$) they gave a

*Corresponding author. Email: jr.kayal@gmail.com

Geomatics, Natural Hazards and Risk
ISSN 1947-5705 Print/ISSN 1947-5713 Online © 2012 Taylor & Francis
http://www.tandf.co.uk/journals
http://dx.doi.org/10.1080/19475705.2011.627380

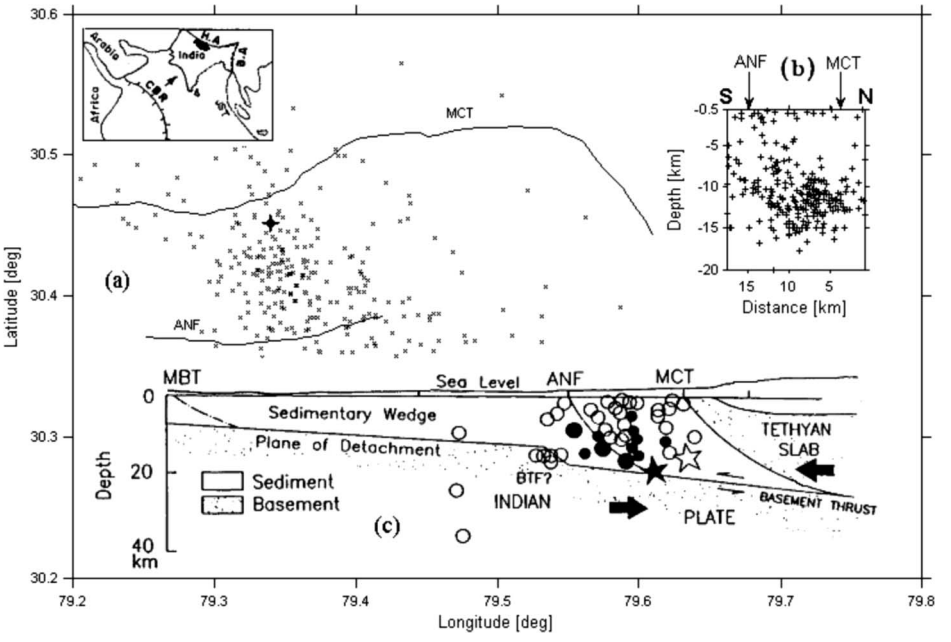

Figure 1. (*a*) The epicentre map of the 1999 Chamoli earthquake sequence. MCT: Main Central Thrust, ANF: Alakananda Fault (Kayal *et al*. 2003b); (*b*) north–south cross-section of the aftershock sequence; (*c*) seismotectonic model of the Chamoli earthquakes recorded by the permanent network within 12 days of the main shock; solid star indicates the IMD and the open star the USGS locations of the main shock (Kayal *et al*. 2003b). Inset: HA: Himalayan Arc, CBR: Carlsberg Ridge, BA: Burmese Arc. The arrow indicates the Indian plate movement.

seismotectonic model showing that the main shock occurred on the plane of detachment at the Alakananda fault (ANF) end at a depth of 15 km. The main shock triggered the ANF to generate the aftershocks (figure 1). They further studied about 350 aftershocks ($M \geq 1.0$) recorded by the eight permanent and about 30 temporary microearthquake seismic stations run by the above organizations, which also fit into this model (Kayal *et al*. 2003b).

In this paper we have considered a total of 348 aftershocks ($M \geq 1.0$), which were recorded by both the permanent and the temporary networks consisting of about 40 seismic stations. The frequency–magnitude relation (*b*-value) and fractal correlation dimension (*D*) are studied to understand the seismic characteristics of the Chamoli earthquake source zone and the seismogenic active fault(s) in the western Himalaya.

2. Tectonic setting of the region

Seismically, the 1999 Chamoli earthquake area in the western Himalaya falls in the MHSB that continues all along the Himalaya within a $\sim$50 km-wide zone between the Main Boundary Thrust (MBT) and the Main Central Thrust (MCT) (Kayal 2001). Most of the moderate-magnitude earthquakes in the western Himalaya

occur at a shallower depth (10–20 km), above the plane of detachment (Seeber *et al*. 1981, Ni and Barazangi 1984, Kayal 2001, 2008). The Indian plate is underthrusting the Eurasian plate along a low-angle (5–15°) thrust plane called the detachment plane (figure 1). In a seismotectonic model of the MHSB, Seeber *et al*. (1981) and Ni and Barazangi (1984) suggested that below the MCT lies the basement thrust front (BTF) or a ramp, the transition zone between the plane of detachment and the basement thrust to the north. They further envisaged that the ramp below the MCT acts as a geometrical asperity for stress concentration for the MHSB earthquakes. The seismotectonic model for the Chamoli earthquake sequence (figure 1(*c*)), however, suggests that the ramp lies to the south of MCT in the Garhwal Himalaya (Kayal 2001, Kayal *et al*. 2003a). The Chamoli area in the Garhwal Himalaya tectonic zone lies to the south of the MCT, where an anticlinal structure is present. This is a part of the large-scale synformal and antiformal structures caused by folding of the south vergent thrust sheets (Valdiya 1976). This schuppen structure is delimited to the south by the east–west-trending ANF that also delimited the high intensity VII isoseismal of the Chamoli main shock (GSI 2001). From the hypocentre location and fault plane solution it has been interpreted that the main shock occurred at the ANF end on the plane of detachment by thrust faulting (Kayal *et al*. 2003a, 2003b) (figure 1). The thrust-faulting solution of the aftershocks to the north of ANF is also comparable with the dipping ANF (Kayal *et al*. 2003b). Seismic characteristics, *b*-value and fractal dimension of this interpreted active fault are examined here.

3. Data analysis

We have used the aftershock data of Kayal *et al*. (2003b) to estimate the frequency–magnitude relation (*b*-value) of the earthquake sequence. These data include the aftershocks recorded by the permanent as well as by the temporary networks for 3 months after the main shock. The aftershock map shows that the events are mostly located within the zone of ANF and MCT (figure 1(*a*)). The north–south cross-section illustrates that the aftershocks are of shallow origin, within a depth range of 0–15 km (figure 1(*b*)). The cross-section of the higher magnitude ($M > 2.5$) aftershocks recorded by the permanent network within 12 days of occurrence of the main shock also shows a similar observation (figure 1(*c*)).

3.1 b-*value*

The *b*-value of these aftershocks is estimated using the Guttenberg and Richter (1944) frequency–magnitude relation: $\log_{10} N = a - bM$, where N is the number of earthquakes in the group having magnitudes larger than M, a and b are constants. The constant '*a*' indicates the seismicity level, and the coefficient '*b*', the slope of the log-linear relation, is known as the *b*-value. The *b*-value varies mostly from 0.5 to 1.5 in a tectonically active region at the plate margins like that in the Himalayas (Kayal 2008). The variability of *b*-values in different tectonic domains may be related to structural heterogeneity and stress distribution in space (Mogi 1962, Scholz 1968). A higher *b*-value means that a smaller fraction of the total earthquakes occur at the higher magnitudes, whereas a lower *b*-value implies a larger fraction occurs at higher magnitudes. In other words, a higher *b*-value indicates lower stress, and a lower *b*-value indicates higher stress in a earthquake source zone (Wyss 1973).

3.2 b-*value mapping*

The *b*-value is estimated by the Maximum Likelihood Method (MLM) given by Aki (1965), which is based on theoretical consideration as:

$$b = (\log e)/(M_a - M_c) \tag{1}$$

where M_a is the average magnitude and M_c is the lower limit or the threshold magnitude, above which the data are complete. We estimated the $M_c = 1.0$ by plotting magnitude and cumulative number of earthquakes. For mapping the spatial variation of the *b*-value, we have divided the aftershock area into small grids of $0.001^\circ \times 0.001^\circ$, and estimated the *b*-value for each grid using the MLM. We used the ZMAP software (Wiemer and Wyss 1997) for computation. The centre of the grid is taken as the plotting point, and thus obtained the *b*-value map of the aftershock area is shown in figure 2(*a*)**.** The map shows a spatial variation of the *b*-value from 0.4–0.7, higher values to the north and lower to the south. The *b*-value is relatively higher in the vicinity of the MCT and it reduces to the south towards the ANF. The average *b*-value for the entire data set is estimated to be about 0.6, which is, however, lower than the normal *b*-value 1.0 for a seismically active region. A north–south cross-section of the *b*-value is then examined; the section is shown in figure 2(*b*).

3.3 *Fractal dimension*

Spatial distribution of earthquakes can be represented by a self-similar mathematical construct, the 'fractal', and the scaling parameter is called the fractal dimension *D* (Mandlebrot 1982). The variability of the fractal dimension in different zones may be related to geological heterogeneity (Aviles *et al*. 1987). It is scale-invariant and is introduced as an efficient statistical parameter to quantify the dimensional distribution of seismicity and, with that, the proportion of randomness and clusterization (e.g. Kagan and Knopoff 1980, Hirata 1989, Ogata 1988, Bhattacharya *et al*. 2002). The fractal dimension is calculated using the correlation integral technique given by Grassberger and Procaccia (1983):

$$D_{wr} = \lim_{r \to 0} (\log(C_r))/(\log_r) \tag{2}$$

where (C_r) is the correlation function. The correlation function measures the spacing or clustering of a set of points, and is given by the relation

$$C(r) = (2/(N(N-1))) \times N(R < r) \tag{3}$$

where $N\ (R < r)$ is the number of pairs (X_i, X_j) with a smaller distance than r. The correlation integral is related to the standard correlation function as given by Kagan and Knopoff (1980):

$$C(r) \sim r^D \tag{4}$$

where D is fractal dimension, more strictly, correlation dimension (here after called D_c). A similar exercise is made to obtain the fractal dimension map using the same grids that are used in *b*-value mapping; the D_c map is shown in figure 3.

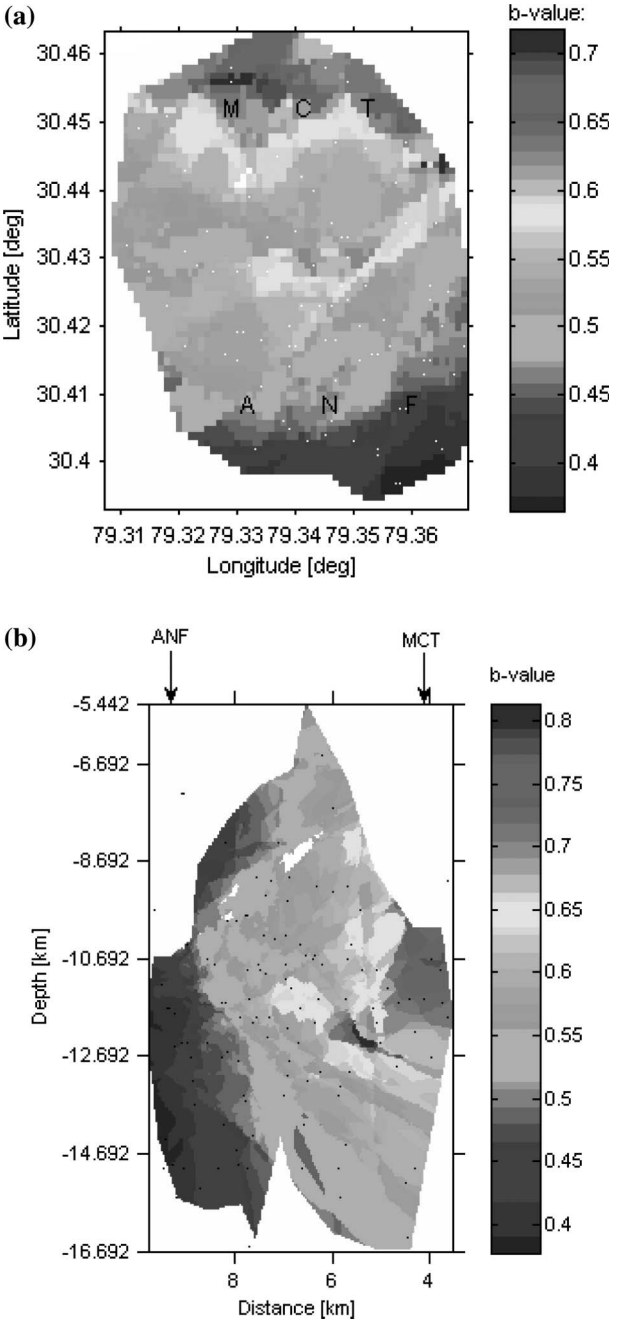

Figure 2. (*a*) *b*-value map of the Chamoli aftershock area; (*b*) north–south cross-section showing the variation of *b*-value with depth.

4. Discussion and conclusions

The *b*-value map of the Chamoli aftershock sequence gives us detailed information about the spatial variation of the frequency–magnitude relation of the Garhwal tectonic zone in the western Himalaya. The seismotectonic model shows that the

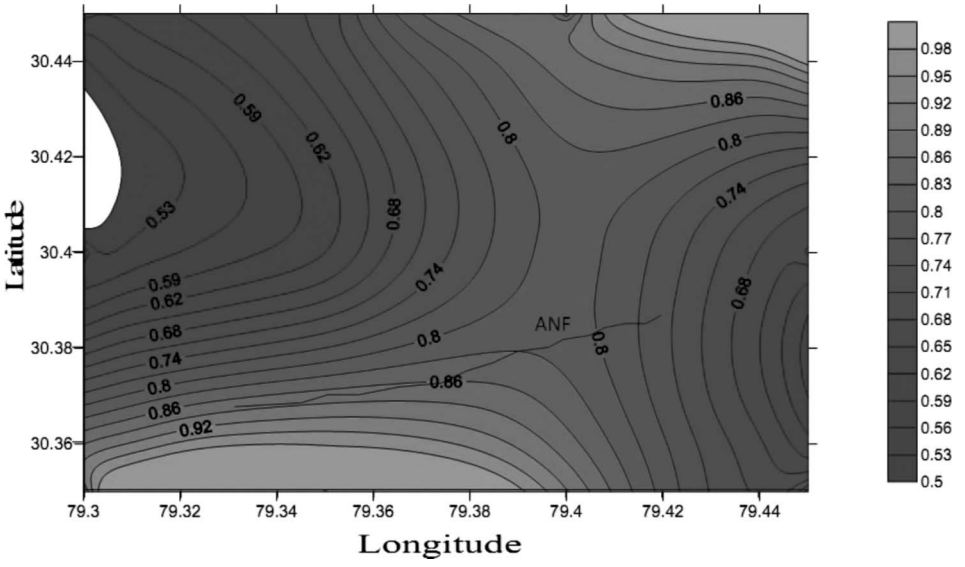

Figure 3. Fractal dimension (D_c) map of the Chamoli aftershock area.

MCT is not the seismogenic fault for the 1999 Chamoli earthquake sequence (figure 1(*c*)). The main shock occurred on the plane of detachment at the ANF end by thrust-faulting, and the ANF was triggered to generate the aftershocks by thrust-faulting (Kayal *et al*. 2003a,b). The spatial as well as depth variation of the *b*-value clearly shows that the ANF zone possesses a lower *b*-value compared with the MCT, which implies that the ANF zone is more stressed than the MCT. Further, the overall *b*-value of the whole aftershock zone is 0.6, which is, however, much lower than the normal value of 1.0 for a seismically active region like that of a continent–continent collision zone in the Himalaya. The lower *b*-value implies that the zone is not only highly stressed, but also that the fraction of higher magnitude earthquakes is greater in this tectonic zone. This observation sheds light on the medium-to-strong earthquake risk in this zone.

Kayal *et al*. (2003a) reported the *b*-value for the aftershock sequence of the first 12 days that was recorded immediately after the main shock by the eight-station local permanent network and found the *b*-value to be 0.57. They also estimated the *b*-value using the temporary network data of about 3 months, 12 days after the main shock, and found it to be 0.61 (Kayal *et al*. 2003b). These observations are comparable with our overall estimate of a *b*-value of 0.6. In addition to the overall estimate of the *b*-value of the aftershock sequence, we have mapped the spatial as well as depth variation of the *b*-value in this study, and the detailed heterogeneities in the tectonic structure in space and depth are imaged (figures 2(*a*) and (*b*)). The seismic characteristics, heterogeneities and vulnerability of the ANF and MCT are depicted in these maps. The ANF is clearly identified not only as an active fault but also as a more stressed zone due to the Himalayan collision tectonics.

The fractal dimension D_c for epicentre distribution characterizes the fault structure. Normally, the D_c ranges from 0–2 (Tosi 1998); when all events cluster into one point, $D = 0$; when homogeneously distributed over a two dimensional embedding space, $D = 2$; and when $D = 1$, this indicates a line source or linear

structure. The estimated fractal dimension contour map shows a linear trend along the ANF with a D_c of 0.8–0.9, but such a trend is absent at the MCT; further north the contours are an artefact as no earthquake is caused by the MCT; the MCT is not the causative fault either for the main shock or for the aftershock sequence (figure 1). The $D_c \sim 0.8$–0.9 at the ANF indicates that the seismogenic ANF is near to a linear structure. The aftershocks are neither clustered at one point nor homogeneously distributed in the source area; the source zone structure may be quantified as $D_c \sim 0.8$–0.9. These seismic characteristics, the frequency–magnitude relation and fractal dimension of the ANF are useful to evaluate the earthquake risk in this tectonic zone.

Acknowledgements

The author AG would like to thank the Department of Science and Technology (DST), Government of India for providing financial assistance for the research work. This work is a part of the Summer Research performed by AG at the Jadavpur University, Kolkata during May–June 2010 under the guidance of JRK.

References

Aki, K., 1965, Maximum-likelihood estimate of b in the formula of log $N = a - bM$ and its confidence limits. *Bulletin Earthquake Research Institute, University of Tokyo*, **43**, pp. 237–239.

Aviles, C.A., Scholz, C.H. and Boatwright, J., 1987, Fractal analysis applied to characteristic segments of the San Andreas fault. *Journal of Geophysical Research*, **92**, pp. 331–344.

Bhattacharya, P.M., Majumdar, R.K. and Kayal, J.R., 2002, Fractal dimension and b-value mapping in northeast India. *Current Science*, **82**, pp. 1486–1491.

Grassberger, P. and Procaccia, I., 1983, Characterisation of strange attractors. *Physics Review Letters*, **50**, pp. 346–349.

Gutenberg, B. and Richter, C.F., 1944, Frequency of earthquakes in California. *Bulletin of the Seismological Society of America*, **34**, pp. 185–188.

GSI, 2001, Chamoli Earthquake of March 29, 1999. *Geological Survey of India Special Publication*, **33**, 170 p.

Hirata, T., 1989, A correlation between the b-value and the fractal dimension of earthquakes. *Journal of Geophysical Research*, **94**, pp. 7507–7514.

IMD, 2000, Chamoli earthquake of March 29, 1999 and its aftershocks, a consolidated document. *Meteorological Monograph, Seismology* **2**, 70 p.

Kagan, Y.Y. and Knopoff, L., 1980, Spatial distribution of earthquakes: The two-point correlation function. *Geophysical Journal of the Royal Astronomical Society*, **62**, pp. 303–320.

Kayal, J.R., 2001, Microearthquake activity in some parts of the Himalaya and the tectonic model. *Tectonophysics*, **339**, pp. 331–351.

Kayal, J.R., 2008, *Microearthquake Seismology and Seismotectonics of South Asia*, 505 p (Berlin: Springer).

Kayal, J.R., Sagina R., Singh, O.P., Chakraborty, P.K. and Karunakar, G., 2003a, The March 1999 Chamoli earthquake in the Garhwal Himalaya: Aftershock characteristics and tectonic structure. *Journal of the Geological Society of India*, **62**, pp. 558–580.

Kayal, J.R., Sagina, R., Singh, O.P., Chakraborty, P.K. and Karunakar, G., 2003b, Aftershock sequence of the March 1999 Chamoli earthquake and the seismotectonic structure of the Garhwal Himalaya. *Bulletin of the Seismological Society of America*, **93**, pp. 109–117.

Mandelbrot, B.B., 1982, *The Fractal Geometry of Nature*, 170 p (San Francisco: Freeman).

Mogi, K., 1962, Magnitude–frequency relations for elastic shocks accompanying fractures of various materials and some related problems in earthquakes. *Bulletin of the Earthquake Research Institute, University of Tokyo*, **40**, pp. 831–853.

Ni, J. and Barazangi M., 1984, Seismotectonics of the Himalayan collision zone: geometry of the under thrusting Indian plate beneath the Himalaya. *Journal of Geophysical Research*, **89**, pp. 1147–1163.

Ogata Y., 1988, Statistical models for earthquake occurrences and residual analysis for point processes. *Journal of the American Statistical Association*, **83**, pp. 9–27.

Seeber, L., Ambruster, J.G. and Quittmeyer, R.C., 1981, Seismicity and continental subduction in the Himalayan arc. In *Zagros, Hindukush, Himalaya Geodynamic Evolution, Geodynamic Series*, **3**, H.K. Gupta and F.M. Delany (Eds), (Washington D.C.: AGU Publications), pp. 215–242.

Scholz C.H., 1968, The frequency–magnitude relation of microfracturing in rock and its relation to earthquakes. *Bulletin of the Seismological Society of America*, **58**, pp. 399–415.

Tosi P., 1998, Seismogenic structure behaviour revealed by spatial clustering of seismicity in the Umbria-Marche Region (Central Italy). *Annals of Geophysics*, **41**, pp. 215–224.

Valdiya K.S., 1976, Himalayan transverse faults and their parallelism with subsurface structures of north Indian plains. *Tectonophysics*, **32**, pp. 352–386.

Wiemer S. and Wyss, M., 1997, Mapping the frequency-magnitude distribution in asperities: An improved technique to calculate recurrence times. *Journal of Geophysical Research*, **102**, pp. 15115–15128.

Wyss, M., 1973, Towards a physical understanding of the earthquake frequency distribution. *Geophysical Journal of the Royal Astronomical Society*, **31**, pp. 341–359.